

# Stochastic Physics-Informed Neural Networks (SPINN): A Moment-Matching Framework for Learning Hidden Physics within Stochastic Differential Equations

Jared O’Leary<sup>a</sup>, Joel A. Paulson<sup>b</sup>, Ali Mesbah<sup>a,\*</sup>

<sup>a</sup>*Department of Chemical and Biomolecular Engineering, University of California,  
Berkeley, Berkeley, 94720, CA, USA*

<sup>b</sup>*Department of Chemical and Biomolecular Engineering, The Ohio State  
University, Columbus, 43210, OH, USA*

---

## Abstract

Stochastic differential equations (SDEs) are used to describe a wide variety of complex stochastic dynamical systems. Learning the hidden physics within SDEs is crucial for unraveling fundamental understanding of these systems’ stochastic and nonlinear behavior. We propose a flexible and scalable framework for training deep neural networks to learn constitutive equations that represent hidden physics within SDEs. The proposed stochastic physics-informed neural network framework (SPINN) relies on uncertainty propagation and moment-matching techniques along with state-of-the-art deep learning strategies. SPINN first propagates stochasticity through the known structure of the SDE (i.e., the known physics) to predict the time evolution of statistical moments of the stochastic states. SPINN learns (deep) neural network representations of the hidden physics by matching the predicted moments to those estimated from data. Recent advances in automatic differentiation and mini-batch gradient descent are leveraged to establish the unknown parameters of the neural networks. We demonstrate SPINN on three benchmark *in-silico* case studies and analyze the framework’s robustness and numerical stability. SPINN provides a promising new direction for systematically unraveling the hidden physics of multivariate stochastic dynamical systems with multiplicative noise.

---

\*Corresponding Author

*Email addresses:* jared.oleary@berkeley.edu (Jared O’Leary), paulson.82@osu.edu (Joel A. Paulson), mesbah@berkeley.edu (Ali Mesbah)

*Keywords:* Stochastic Differential Equations, Moment-Matching, Hidden Physics, Deep Neural Networks, Uncertainty Propagation

---

## 1. Introduction

Stochastic dynamical systems are ubiquitous in a wide range of science and engineering problems, such as dynamical systems governed by Brownian motion or those that experience random perturbations from their surrounding environment [1, 2, 3, 4, 5]. Stochastic differential equations (SDEs) are used to describe the complex behavior of a wide variety of stochastic dynamical systems, including those involving electrical and cell signal processing [6, 7, 8], colloidal/molecular self-assembly [9, 10, 11, 12], nucleation processes [13, 14], and predator-prey dynamics [15, 16]. An important challenge in constructing and studying SDEs is that they often contain physics that are either unknown (e.g., a population density-dependent transmission function for disease spread [17, 18] or a weather-dependent tire road friction coefficient [19]), or cannot be directly measured (e.g., free energy and diffusion landscapes [9, 10, 11, 12]). Creating a systematic framework to learn the hidden physics within SDEs is thus crucial for unraveling fundamental understanding of stochastic dynamical systems.

A widely used form of SDEs is given by:

$$dx = f(x, g(x))dt + h(x, g(x))dw, \quad (1)$$

where  $x$  is the system state,  $t$  is the time, and  $w$  is a Gaussian white noise process. The “modeled” or “known” physics is comprised of  $f$ ,  $h$ , and the structure of the SDE (i.e., the additive relationship between  $f$  and  $h$  and the multiplicative relationship between  $h$  and  $w$ ), while  $g$  is the “unmodeled” or “unknown” hidden physics. Note that when  $g(x) = [g_1(x), g_2(x)]^\top$  and  $f$  and  $h$  are identity functions, Eq. 1 reduces to the following:

$$dx = g_1(x)dt + g_2(x)dw. \quad (2)$$

Despite extensive literature on the subject [20, 21, 22, 23, 24, 25, 26, 27], the vast majority of methods for learning hidden physics within SDEs require *a priori* knowledge about the stochastic system, are intractable for multi-dimensional systems, may not be suitable for recovering highly nonlinear and state-dependent versions of  $g$ , or rely on inflexible and system-specific sampling techniques.

We seek to investigate strategies based on deep learning to create a flexible and scalable framework for systematically learning the hidden physics within SDEs of form (1). To this end, we first propose approximating  $g(x)$  as a (deep) artificial neural network, where the weights and biases within the neural network represent the SDE hidden physics. To our knowledge, all previous methods for learning SDE hidden physics either (i) learn  $g(x)$  at discrete values of  $x$  and then fit analytic functions to these discrete values [20, 21, 22, 24, 26, 27], or (ii) approximate  $g(x)$  using basis functions and learn the coefficients of those basis functions [23, 25]. The former approach can become intractable when the dimension of  $x$  is large, or when  $g(x)$  is highly nonlinear and thus requires  $x$  to be finely discretized. The latter approach can be extremely sensitive to the choice of basis functions and exhibits other numerical issues. Artificial neural networks, on the other hand, provide a scalable and flexible way of approximating a highly nonlinear relationship between  $g(x)$  and (continuous values of)  $x$  without the need for *a priori* assumptions about the form of that relationship [28, 29, 30].

We next propose combining the recently developed notion of physics-informed neural networks [31, 32, 33, 34, 35] and moment-matching [36, 37, 38] to learn the weights and biases within the neural network that approximates  $g(x)$ . The key idea behind physics-informed neural networks is that constraining loss functions with differential equations that govern underlying system physics (e.g., conservation of momentum) can enhance the robustness and efficiency of training neural networks. Physics-informed neural networks have also been shown to enable discovery of constitutive equations from incomplete models and data [31, 32, 33]. In this work, we apply established uncertainty propagation techniques (e.g., linearization [39, 40], unscented transform [41, 42]) to the known structure of the SDE to predict the time evolution of the statistical moments of the stochastic states for fixed neural network weights and biases. Note that these predicted moments are a function of both the known and hidden SDE physics. We construct a loss function that matches these (physics-informed) predicted moments to moments that are estimated from system trajectory data. We learn the neural network weights and biases by implementing an efficient training algorithm that leverages recent advances in automatic differentiation and mini-batch gradient descent [43, 44].

Integrating uncertainty propagation techniques directly into the proposed framework allows the framework to predict the time evolution of an arbitrary number of moments (e.g., mean, variance, skew, kurtosis trajectories) over

time intervals of arbitrary size. Although other reported approaches for learning SDE hidden physics involve moment calculations [20, 24, 26, 27], these methods (i) sample stochastic states at extremely small time intervals, (ii) involve system-specific interpolation techniques, and/or (iii) are limited to calculating only the first two moments. Moreover, the proposed framework can naturally incorporate different uncertainty propagation techniques, including linearization, unscented transform, generative adversarial networks, and polynomial chaos [33, 34, 39, 40, 41, 42, 45]. Furthermore, the use of mini-batch gradient descent to learn the weights and biases within the neural network approximation of  $g(x)$  does not require any assumptions regarding the shape or smoothness of  $g(x)$ , whereas previously reported methods based on Bayesian inference rely on such assumptions [22, 23].

We demonstrate this stochastic physics-informed neural network framework (SPINN) on three benchmark *in-silico* case studies. The dynamics of each system are described by SDEs of form (1) that contain nonlinear and state-dependent hidden physics terms. The first case study is a one-state model for directed colloidal self-assembly with an exogenous input [46], the second is a two-state competitive Lotka-Volterra model with a coexistence equilibrium [47], and the third is a three-state susceptible-infectious-recovered (SIR) epidemic model for disease spread [48]. We show that SPINN is able to learn the hidden physics within these SDEs with high accuracy. We finally analyze the robustness and numerical stability of SPINN in light of practical considerations such as data collection and computing time. SPINN is available on GitHub with end-to-end examples [49].

## 2. Methods

Fig. 1 gives a schematic overview of SPINN. Repeated stochastic dynamical system trajectories are recorded to estimate the time evolution of statistical moments of the stochastic state  $m_x^{(ij)}(t_k)$  (left). The hidden physics  $g(x)$  are represented by a neural network that is parameterized by unknown weights and biases  $\theta$  (center). Uncertainty propagation techniques are applied to Eq. (1) to predict the moment time evolution for fixed neural network parameters,  $\hat{m}_x^{(ij)}(t_k)$  (left to center). A loss function is constructed using the predicted and data-estimated moments (center). Mini-batch gradient descent is used to update the parameters  $\theta$  within  $g(x; \theta)$  by minimizing the loss function (right). The hidden physics,  $g(x; \theta)$ , are considered “learned” once the mini-batch gradient descent algorithm converges. The subsequent sections

describe in more detail how data is collected and how SPINN uses uncertainty propagation, moment-matching, and mini-batch gradient descent to learn the weights and biases within the neural networks that approximate the unknown hidden physics within SDEs.

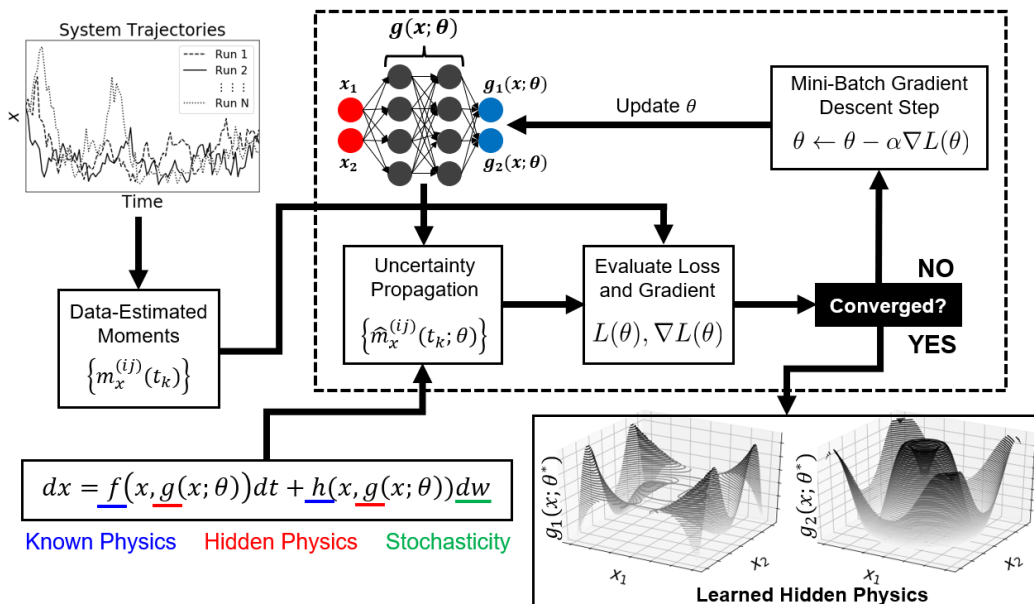


Figure 1: Stochastic physics-informed neural network framework (SPINN) summary. The key steps include (i) estimating the time evolution of statistical moments  $m_x^{(ij)}(t_k)$  from repeated stochastic dynamical system trajectories, (ii) approximating the hidden physics as a neural network (e.g.,  $g(x; \theta) = [g_1(x; \theta), g_2(x; \theta)]^\top$ , where the unknown weights and biases are  $\theta$ ), (iii) applying uncertainty propagation techniques to the known structure of the stochastic differential equation to predict the time evolution of statistical moments  $\hat{m}_x^{(ij)}(t_k)$ , and (iv) using moment-matching and mini-batch gradient descent to learn “optimal” weights and biases  $\theta^*$ .

### 2.1. Data Collection

Data collection is accomplished by repeating stochastic dynamical system trajectories starting from identical initial conditions. Here,  $N + 1$  trajectories start from some initial condition  $x_0$ . During each trajectory, state values  $x$  are recorded at time points  $t_k$  for  $K + 1$  total time steps. The  $N + 1$  recorded values of each  $x(t_k)$  are used to estimate moments  $m_x^{(ij)}(t_k)$ . In this work, we only record the first two moments, the mean,  $\mu_x(t_k)$ , and the covariance,  $\Sigma_x(t_k)$ . SPINN can naturally accommodate more moments, however, and

doing so can potentially lead to more accurate recovery of the hidden physics. The data-estimated means and covariances are calculated from:

$$\begin{aligned}\mu_x(t_k) &= \frac{1}{N+1} \sum_{n=0}^N x_n(t_k) \\ \Sigma_x(t_k) &= \frac{1}{N} \sum_{n=0}^N (\mu_x(t_k) - x_n(t_k))(\mu_x(t_k) - x_n(t_k))^\top,\end{aligned}\quad (3)$$

where  $n$  is the trajectory index between 0 and  $N$ .

Repeated stochastic trajectories from only one initial condition often do not explore a large percentage of the state space. As a result, the stochastic trajectories can be collected from various unique initial conditions. In this work, we choose initial conditions by performing a grid search within a range of state values of interest. We note, however, that more efficient sampling techniques can also be used [50, 51, 52, 53, 54].

The data-estimated means and covariances  $\mu_x(t_k)$  and  $\Sigma_x(t_k)$  are collected at discrete time points. In order to perform moment-matching, the SDE must be discretized accordingly. When  $h$  in Eq. (1) is not a function of  $x$ , the noise is said to be “additive” and different discretization schemes will lead to one unique stochastic process [55, 56]. However, when  $h$  is a function of  $x$ , the noise is said to be “multiplicative”. Here, different discretization schemes will lead to different stochastic processes.

The two most common discretization conventions are the Ito convention, where the value of  $x$  just before the white noise jump is used in  $h(x, g(x))$  and the Stratonovich convention, where  $x$  is taken to be half of the sum of the values before and after the jump [55, 56]. The Ito convention is generally used for dynamic modeling because it is easier to manipulate and does not assume any knowledge of the future as  $h(x, g(x))$  is evaluated before the jump only. The Ito convention is compatible with explicit Euler discretization, and the corresponding Euler-Maruyama discretization scheme is employed throughout this work [57, 58]. Note that SPINN can in principle accommodate “higher-order” Ito discretization methods (e.g., Milstein [59]), but the exploration of such methods is beyond the scope of this work. The form of Eq. (1) after Euler-Maruyama discretization is shown below:

$$\begin{aligned}x(t_k) &= M(x(t_{k-1})) \\ &= x(t_{k-1}) + \Delta t f(x(t_{k-1}), g(x(t_{k-1}))) \\ &\quad + w(t_{k-1})h(x(t_{k-1}), g(x(t_{k-1})))\sqrt{\Delta t}.\end{aligned}\quad (4)$$

## 2.2. Uncertainty Propagation

We apply unscented transform (UT) [40, 41, 42] to Eq. (4) to propagate stochasticity through the system dynamics, which in turn yields the time evolution of the mean and covariance. The predicted mean and covariance  $\hat{\mu}_x(t_k)$  and  $\hat{\Sigma}_x(t_k)$  are functions of the hidden physics,  $g$ , the known physics,  $f$  and  $h$ , the known structure of the SDE, and data-estimated means and covariances at previous time points,  $\mu_x(t_{k-1})$  and  $\Sigma_x(t_{k-1})$ . UT uses  $\mu_x(t_{k-1})$  and  $\Sigma_x(t_{k-1})$  to calculate  $2p+1$  sigma points, where  $p$  is the dimension of the uncertainty. These sigma points,  $\mathcal{X}$ , represent the distribution of  $x(t_{k-1})$  and are created by a function  $q$ . The sigma points are then propagated through the dynamics of Eq. (4) and subsequently weighted with weights  $W$ . The mean and covariance of these nonlinearly transformed and weighted sigma points are  $\hat{\mu}_x(t_k)$  and  $\hat{\Sigma}_x(t_k)$ . We note that  $q$  and  $W$  depend on heuristic-based scaling values [40, 41, 42]. Identical, standard choices of these scaling values were used in each of the case studies in this work. The UT algorithm is summarized below:

1. Create  $2p + 1$  sigma points:

$$\mathcal{X}(t_{k-1}) = q(\mu_x(t_{k-1}), \Sigma_x(t_{k-1}))$$

2. Propagate sigma points through Eq. (4):

$$\mathcal{X}(t_k) = M(\mathcal{X}(t_{k-1}))$$

3. Predict mean:

$$\hat{\mu}_x(t_k) = \sum_{l=0}^{2p} W_l \mathcal{X}_l(t_k)$$

4. Predict covariance:

$$\hat{\Sigma}_x(t_k) = \sum_{m=0}^{2p} W_m (\mathcal{X}_m(t_k) - \hat{\mu}_x(t_k)) (\mathcal{X}_m(t_k) - \hat{\mu}_x(t_k))^\top$$

The prediction scheme outlined above only predicts the mean and covariance one step forward in time (i.e.,  $\hat{\mu}_x(t_k)$  and  $\hat{\Sigma}_x(t_k)$  from  $\mu_x(t_{k-1})$  and  $\Sigma_x(t_{k-1})$ ). UT is capable of predicting means and covariances to an arbitrary number of time steps in the future from data-estimated moments  $\mu_x(t_{k-1})$  and  $\Sigma_x(t_{k-1})$ . In this work, data-estimated moments are available at every time step  $t_k$ . As a result, only one-step predictions are used within SPINN to learn

the hidden physics. SPINN can, however, accommodate multi-step moment predictions via UT (or other uncertainty propagation schemes). This would be useful in scenarios where data-estimated moments are sparsely available.

Although SPINN can accommodate other uncertainty propagation techniques, UT holds key advantages over many established methods in terms of computational cost, accuracy, and ease of implementation [40, 41, 42]. The UT method requires  $2p + 1$  function evaluations, which scale linearly with respect to the uncertainty dimension  $p$ . This method can thus be substantially less expensive than general sample-based methods (e.g., Monte Carlo methods [60]) that typically require orders of magnitude more sample points for accurate computation of  $\hat{\mu}_x(t_k)$  and  $\hat{\Sigma}_x(t_k)$ . Moreover, linearization techniques can diverge for systems that are highly nonlinear and require (potentially expensive) Jacobian calculations [40, 41]. Other established techniques for uncertainty propagation through SDEs (e.g., generative adversarial networks [33] and polynomial chaos [45]) can be difficult to implement and can sometimes require complex, system-specific choices (e.g., finite truncation in polynomial chaos). UT, on the other hand, is simple to implement as it requires only a selection of sigma points and simple mean and covariance calculations. Most importantly, UT only requires the deterministic part of Eq. 4 (i.e.,  $f(x(t_{k-1}), g(x(t_{k-1})))$ ) to predict the mean  $\hat{\mu}_x(t_k)$ . This allows SPINN to learn the hidden physics within  $f$  and  $h$  sequentially, which significantly simplifies the framework’s numerics, as described in the next section.

### 2.3. Moment-Matching via Mini-Batch Gradient Descent

The hidden physics  $g(x)$  can be represented by a neural network that is parameterized by weights and biases  $\theta$  (i.e.,  $g(x; \theta)$ ), where weight and bias values  $\theta^*$  denote the optimal parameters of the neural network. As discussed above, predicted moments  $\hat{\mu}_x(t_k)$  and  $\hat{\Sigma}_x(t_k)$  are functions of  $f$ ,  $h$ ,  $g$ , the known structure of the SDE, and sigma points  $\mathcal{X}$ , which in turn are functions of the data-estimated moments,  $\mu_x(t_{k-1})$  and  $\Sigma_x(t_{k-1})$ . We find  $\theta^*$  (and thus train  $g(x; \theta)$ ) by minimizing the distance between  $K + 1$  estimated and predicted moments. The moment-matching problem is formulated as:

$$\min_{\theta} \sum_{k=0}^K \left\| \hat{\mu}_x(t_k) - \mu_x(t_k) \right\|^2 + \left\| \hat{\Sigma}_x(t_k) - \Sigma_x(t_k) \right\|^2. \quad (5)$$

We reiterate that although Eq. (5) is written in terms of only the first two moments, SPINN can naturally accommodate more moments. We further re-

iterate that the predicted moments  $\hat{\mu}_x(t_k)$  and  $\hat{\Sigma}_x(t_k)$  are one-step predictions determined from  $\mu_x(t_{k-1})$  and  $\Sigma_x(t_{k-1})$ .

A key advantage of using UT for propagating stochasticity through Eq. (1) is that  $h$  does not contribute to mean predictions  $\hat{\mu}_x(t_k)$ ; although both  $f$  and  $h$  contribute to covariance predictions  $\hat{\Sigma}_x(t_k)$ . This allows us to train separate neural networks that represent the hidden physics within  $f$  and  $h$ . Instead of training one neural network  $g(x; \theta)$  that represents the hidden physics within  $f$  and  $h$ , we can sequentially train two separate neural networks  $g_1(x; \theta_1)$  and  $g_2(x; \theta_2)$  that represent the hidden physics within  $f$  and  $h$ , respectively. This sequential training helps prevent the framework from finding “degenerate” solutions of Eq. (5) (i.e., parameters  $\theta^*$  that lead to accurate reconstructions of  $\mu_x(t_k)$  and  $\Sigma_x(t_k)$  but do not accurately reflect the system’s hidden physics). Thus, when UT is used, SPINN finds  $g_1(x; \theta_1^*)$  by solving Eq. (6):

$$\min_{\theta_1} \sum_{k=0}^K \|\hat{\mu}_x(t_k) - \mu_x(t_k)\|^2. \quad (6)$$

Subsequently, SPINN uses  $g_1(x; \theta_1^*)$  to determine  $g_2(x; \theta_2^*)$  via:

$$\min_{\theta_2} \sum_{k=0}^K \|\hat{\Sigma}_x(t_k) - \Sigma_x(t_k)\|^2. \quad (7)$$

We solve Eqs. (6)-(7) by leveraging recent advances in automatic differentiation and mini-batch gradient descent [43, 44, 61]. Here, the collected data (i.e.,  $K + 1$  data-estimated moments) is split into training, validation, and testing datasets at a 60%/20%/20% ratio. During training, the mean squared error (MSE) of a “mini-batch” of predicted moments from Eqs. (6)-(7) is used to iteratively update  $\theta_{1,2}$  until  $\theta_{1,2}$  converges to  $\theta_{1,2}^*$ . The validation data is used to assess whether  $\theta_{1,2}$  has converged (via “early-stopping” [62]) while the test data is used to evaluate the performance of the fully trained neural networks  $g_1(x; \theta_1^*)$  and  $g_2(x; \theta_2^*)$ . All neural networks used in this work have identical and standard architectural choices, which include: a mini-batch size of 32 predicted moments [61], the use of Adam optimizer with a learning rate of  $1e-4$  [63], Swish activation functions in hidden layers [64], and linear activation functions in output layers. Neural network size (i.e., number of hidden layers/nodes) can vary among case studies, but Section 3.2 shows that many network sizes yield similar performance. All of the code used in this work is written in the Tensorflow API Keras [44, 65] and is available on GitHub [49].

### 3. Results and Discussion

We demonstrate SPINN on three benchmark *in-silico* case studies from the literature: (i) a one-state model for directed colloidal self-assembly with an exogenous input [46], (ii) a two-state competitive Lotka-Volterra model with a coexistence equilibrium [47], and (iii) a three-state SIR epidemic model for disease spread [48]. Each of these stochastic dynamical systems can be modeled by Eq. (1). State trajectory data is collected according to the approach described in Section 2.1 and the SPINN framework outlined in Sections 2.2–2.3 is used to learn (or reconstruct) the hidden physics. SPINN’s performance is evaluated by assessing the accuracy of the reconstructed hidden physics.

In each case study, data-estimated means and covariances  $\mu_x(t_k)$  and  $\Sigma_x(t_k)$  are calculated from  $10^5$  replicates of 50 time-step state trajectories from 2000 unique initial conditions (meaning  $N + 1 = 10^5$  and  $K + 1 = 50 \times 2000$ ). As mentioned in Section 2.1, the number of initial conditions could very likely be decreased by employing more advanced sampling strategies, but exploring such strategies is beyond the scope of this work. Section 3.3 examines the relationship between the number of trajectory replicates and hidden physics reconstruction accuracy.

#### 3.1. Case Study 1: Directed Colloidal Self-Assembly

The first case study is a one-state model for directed colloidal self-assembly with an an exogenous input [46]. Here, the voltage of an external electric field is adjusted to mediate the two-dimensional self-assembly of silica micro-particles. The system dynamics are modeled according to Eq. (1). Denote  $x$  as an order parameter that represents crystal structure (i.e., the system state),  $u$  as the electric field voltage (i.e., the exogenous input),  $K$  as Boltzmann’s constant, and  $T$  as the temperature:

$$\begin{aligned} \frac{dx}{dt} &= g_1(x, u) + w(t)\sqrt{2g_2(x, u)} \\ g_1(x, u) &= \frac{d}{dx}\left(g_2(x, u)\right) - \frac{d}{dx}\left(F(x, u)\right)\frac{g_2(x, u)}{KT} \\ g_2(x, u) &= 4.5 \times 10^{-3}e^{-(x-2.1-0.75u)^2} + 0.5 \times 10^{-3} \\ F(x, u) &= 10KT(x - 2.1 - 0.75u)^2. \end{aligned} \tag{8}$$

The hidden physics are the drift coefficient,  $g_1(x, u)$ , and the diffusion coefficient,  $g_2(x, u)$ . Note that  $g_1(x, u)$  is a function of a  $g_2(x, u)$  and the free

energy landscape  $F(x, u)$ . This relationship provides an example of how drift and diffusion coefficients can be used to derive other hidden system physics.

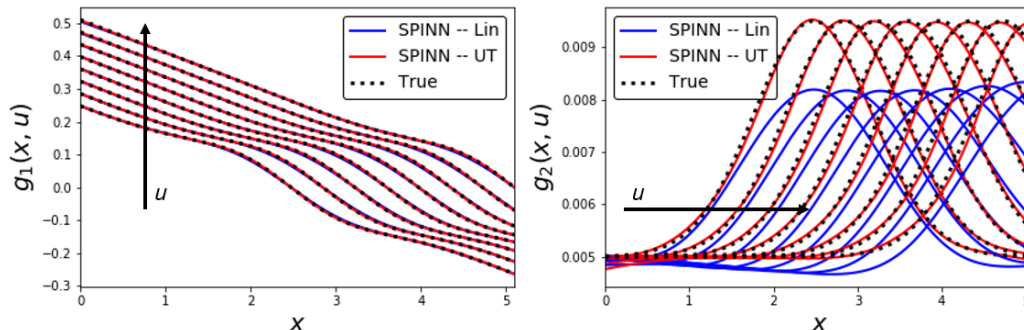


Figure 2: Learned hidden physics of directed colloidal self-assembly system. Using unscented transform (UT) and linearization (Lin) for uncertainty propagation, SPINN learns the drift and diffusion coefficients  $g_1(x, u)$  and  $g_2(x, u)$  of the stochastic dynamical system described by Eq. (8). SPINN with UT reconstructs both  $g_1(x, u)$  and  $g_2(x, u)$  with high accuracy. While UT and Lin yield similar reconstructions of  $g_1(x, u)$ , UT significantly outperforms Lin in the reconstruction of  $g_2(x, u)$ .

We chose this case study because the hidden physics are highly nonlinear and depend on an exogenous input. To our knowledge, no previously reported approach for learning SDE hidden physics has explicitly learned  $g(x, u)$ . Instead, existing approaches typically seek to learn  $g(x)$  at discrete values of  $u$  and interpolate [9, 10, 11, 12, 46]. This requires repeating the entire hidden physics learning procedure for many discrete values of  $u$  and, thus, demands a trade-off between computational cost and accuracy. SPINN, on the other hand, directly learns  $g(x, u)$  over the entire  $(x, u)$  state space.

Fig. 2 shows SPINN’s reconstruction of  $g_1(x, u)$  and  $g_2(x, u)$  when using UT and linearization for uncertainty propagation. SPINN with UT learns  $g_1(x, u)$  and  $g_2(x, u)$  with high accuracy. While UT and linearization yield similar reconstructions of  $g_1(x, u)$ , UT significantly outperforms linearization in the reconstruction of  $g_2(x, u)$ . The reconstruction root mean squared errors (RMSEs) for  $g_1(x, u)$  and  $g_2(x, u)$  are reported in Table 1 in Section 4.

Fig. 3 compares how effectively UT and linearization propagate stochasticity through Eq. (8). Here, each uncertainty propagation strategy takes data-estimated moments  $\mu_x(t_{k-1})$  and  $\Sigma_x(t_{k-1})$  from the test dataset as an input and predicts moments at the next time step  $\hat{\mu}_x(t_k)$  and  $\hat{\Sigma}_x(t_k)$ . The one-step moment prediction RMSEs are then shown as histograms. Although the UT and linearization yield similar one-step predictions for the mean, lin-

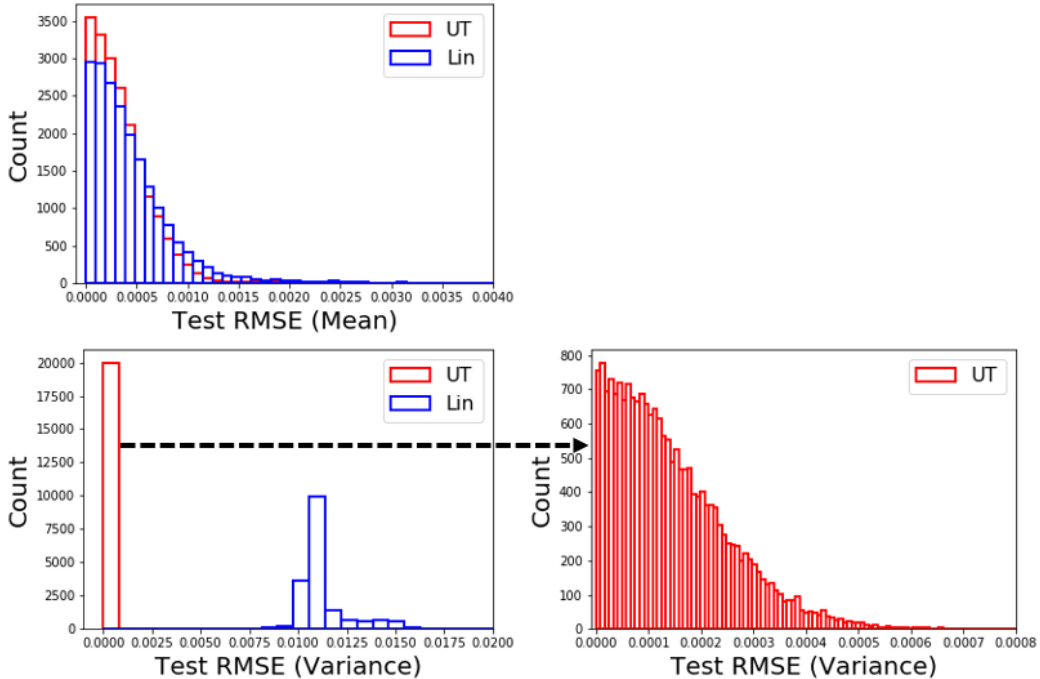


Figure 3: Uncertainty propagation strategy comparison. Unscented transform (UT) and linearization (Lin) propagate stochasticity through Eq. (8). Each strategy takes data-estimated means and variances  $\mu_x(t_{k-1})$  and  $\Sigma_x(t_{k-1})$  from the test dataset (see Section 2.3) as an input and predicts the means and variances at the next time step  $\hat{\mu}_x(t_k)$  and  $\hat{\Sigma}_x(t_k)$ . The root mean squared errors (RMSEs) of the one-step predictions of the means variances are shown as histograms. The histogram on the right is the zoomed-in version of the RMSE of UT’s one-step variance predictions.

earization leads to poor one-step predictions of the variance in comparison to UT. This result is expected for systems with highly nonlinear dynamics [40, 41, 42]. Moreover, this result is consistent with the results in Fig. 2, as variance predictions are required to learn  $g_2$  but not to learn  $g_1$ . Although the choice of uncertainty propagation technique certainly affects the ability of SPINN to learn hidden physics, the framework can accommodate many uncertainty propagation techniques. UT has been shown to successfully propagate uncertainty (or stochasticity) through many complex systems and is used for uncertainty propagation throughout the remainder of this work. UT is also automatically embedded in the GitHub code [49].

### 3.2. Case Study 2: Competitive Lotka-Volterra with Coexistence Equilibrium

The second case study is a two-state competitive Lotka-Volterra model with a coexistence equilibrium [47]. The stochastic dynamics are modeled according to Eq. (1). Note that  $x = [x_1, x_2]^\top$  and  $x_i^{\text{eq}}$  are the coexistence equilibrium points:

$$\begin{aligned}
 \frac{dx_1}{dt} &= g_1(x)_1 + w_1(t)\sqrt{2g_2(x)_1} \\
 \frac{dx_2}{dt} &= g_1(x)_2 + w_2(t)\sqrt{2g_2(x)_2} \\
 g_1(x)_1 &= x_1(1 - x_1 - k_1x_2) \\
 g_1(x)_2 &= x_2(1 - x_2 - k_2x_1) \\
 g_2(x)_1 &= x_1(x_2 - x_2^{\text{eq}}) \\
 g_2(x)_2 &= x_2(x_1 - x_1^{\text{eq}}) \\
 x_1^{\text{eq}} &= \frac{1 - k_1}{1 - k_1k_2}, \quad x_2^{\text{eq}} = \frac{1 - k_2}{1 - k_1k_2} \\
 k_1 &= 0.4, \quad k_2 = 0.5.
 \end{aligned} \tag{9}$$

The hidden physics are the two-dimensional drift and diffusion coefficients,  $g_1(x_1, x_2)$  and  $g_2(x_1, x_2)$ . As a result, we seek to train two multi-input, multi-output neural networks that approximate the hidden physics. The drift coefficient neural network takes  $x_1$  and  $x_2$  as input and outputs  $g_1(x_1, x_2)_1$  and  $g_1(x_1, x_2)_2$ . The diffusion coefficient neural network takes  $x_1$  and  $x_2$  as input and outputs  $g_2(x_1, x_2)_1$  and  $g_2(x_1, x_2)_2$ .

We chose this case study because both the drift and diffusion coefficients are multi-dimensional and nonlinear. We apply SPINN to this “more complex” SDE to demonstrate the framework’s scalability. Note that no aspect of the framework was altered from its implementation in the previous section. Further, although other reported approaches have learned SDE hidden physics of similar complexity, these approaches suffer from the drawbacks mentioned in Section 1; these include (i) learning  $g(x)$  at discrete values of  $x$  and then fitting analytic functions to these values and (ii) requiring complex, system-specific sampling techniques [9, 20, 24, 26, 27].

Fig. 4 shows SPINN’s reconstruction of  $g_1(x_1, x_2)_1$ ,  $g_1(x_1, x_2)_2$ ,  $g_2(x_1, x_2)_1$ , and  $g_2(x_1, x_2)_2$ . SPINN learns all four terms with high accuracy and reconstruction RMSEs for each term are reported in Table 1 in Section 4. Fig. 5 examines the sensitivity of mini-batch gradient descent to (i) the neural network sizes of  $g_i(x_1, x_2; \theta)$  (i.e., number of hidden nodes and layers) and (ii) the

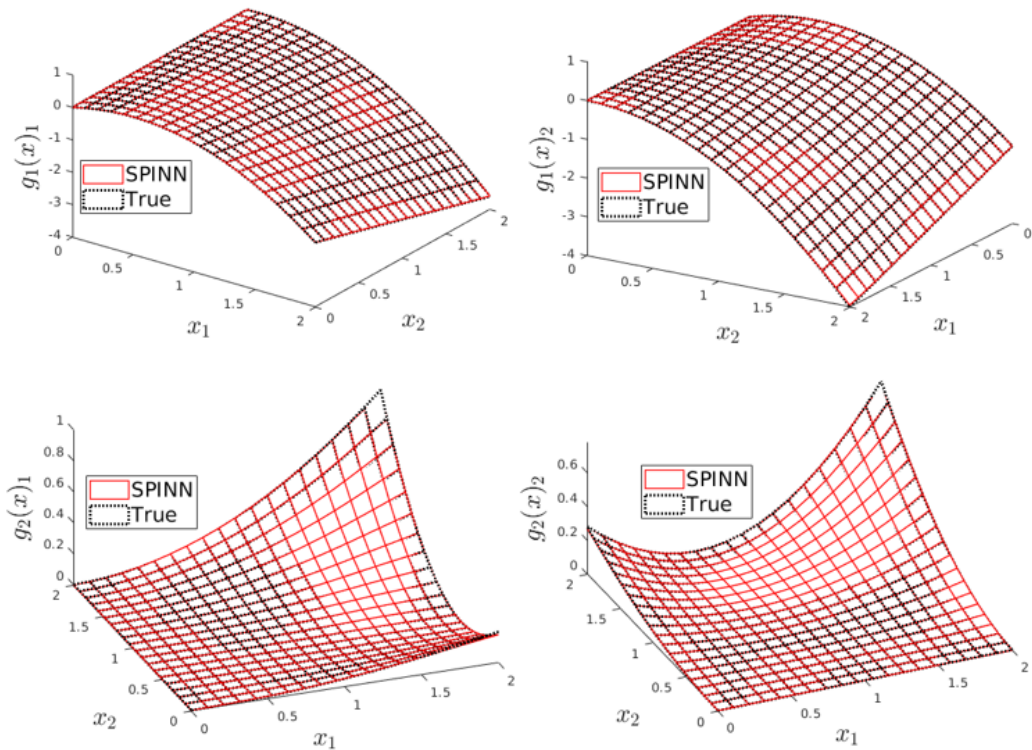
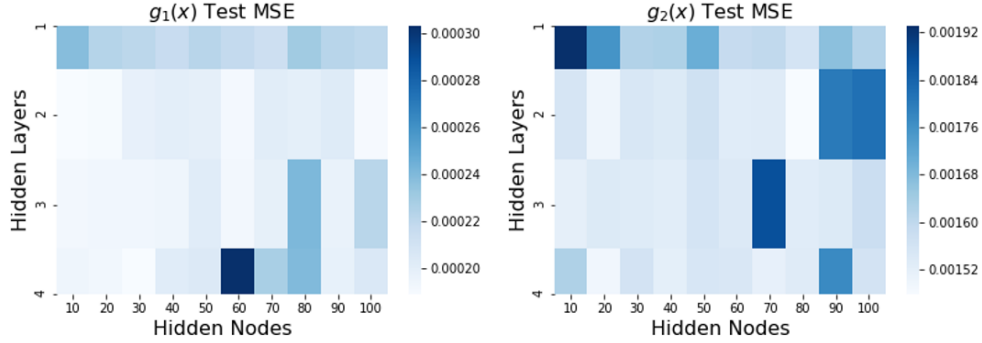
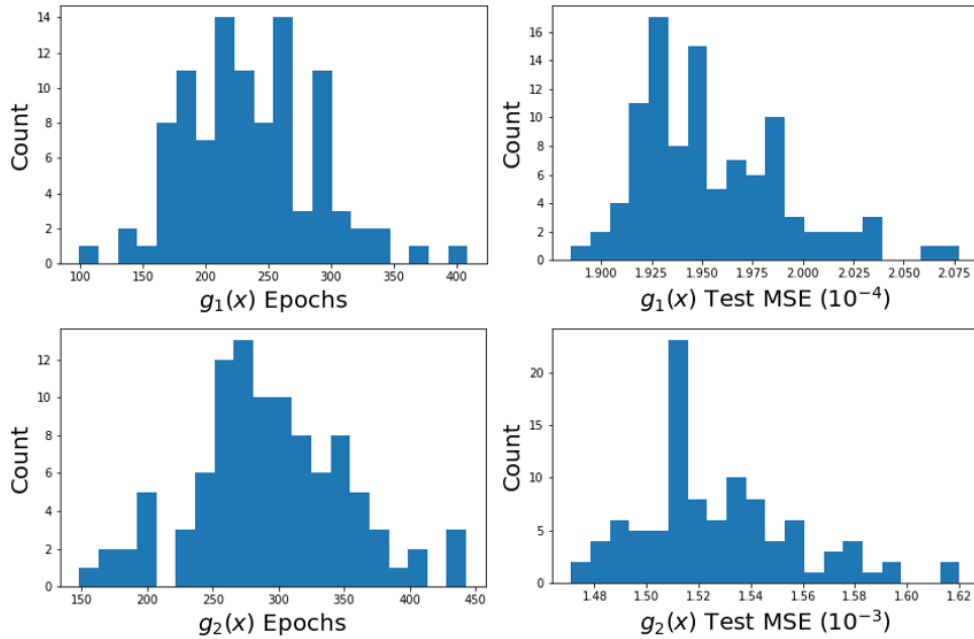


Figure 4: Learned hidden physics of competitive Lotka-Volterra system with coexistence equilibrium. SPINN reconstructs  $g_1(x_1, x_2)_1$ ,  $g_1(x_1, x_2)_2$ ,  $g_2(x_1, x_2)_1$  and  $g_2(x_1, x_2)_2$  with high accuracy.

initial values of weights  $\theta$ . Although other hyper-parameters within SPINN (e.g., learning rate, batch size) can affect the gradient descent, the values of these parameters are fairly standardized and not expected to change with separate implementations of the framework [28, 29, 30, 61, 64, 63]. On the other hand, neural network size can change significantly based on the complexity of the hidden physics and weight values are semi-randomly initialized every time a neural network is trained. Fig. 5a shows a heat map that matches the test MSE with network size for  $g_1(x_1, x_2)$  and  $g_2(x_1, x_2)$ . The figure shows that many network sizes yield similar performance and suggests that mini-batch gradient descent is fairly robust towards this hyper-parameter. This serves as a first pass demonstration of SPINN’s convergence stability. Note that Bayesian optimization approaches can be used along with SPINN to eliminate the need for manual hyper-parameter selection [66].



(a) Network size sensitivity analysis.



(b) Weight initialization sensitivity analysis.

Figure 5: (a) SPINN learns hidden the physics  $g_1(x_1, x_2)$  and  $g_2(x_1, x_2)$  of Eq. (9) under a variety of network sizes. The heat map matches the test dataset mean squared error (MSE) with network size and shows that many network sizes yield similar performance. (b) The  $g_1(x)$  neural network contains 2 hidden layers and 10 nodes per layer. The  $g_2(x)$  neural network contains 2 hidden layers and 20 nodes per layer. These neural networks are trained 100 times with different initial weights and histograms of the test MSE and number of epochs are shown. The histograms demonstrate that the test MSE is consistent among runs while the number of epochs required to reach that MSE varies significantly.

For  $g_1(x_1, x_2)$  and  $g_2(x_1, x_2)$ , the “optimal” network sizes are those with 2 hidden layers and 10 and 20 nodes, respectively. These network sizes are used to produce the results shown in Fig. 4. The selected neural networks are next trained 100 times with different initial weights. Fig. 5b shows histograms of the test MSE and the number of epochs for each run. Note that the number of epochs varies because the neural networks are trained using early-stopping. Here, training ends once the validation error begins to increase [62]. The histograms show that the test MSE is consistent among runs while the number of epochs required to reach that MSE varies significantly. We do not view the variation in epoch number (or training time) as evidence of the mini-batch gradient descent’s lack of convergence stability, but instead as an unavoidable byproduct of the randomized weight initialization.

### 3.3. Case Study 3: Susceptible-Infectious-Recovered Epidemic Model

The third case study is a three-state SIR epidemic model for disease spread [48]. The stochastic dynamics are modeled according to Eq. (1):

$$\begin{aligned}
\frac{dS}{dt} &= b - dS - g(S, I) + \gamma R + \sigma_1 S w_1(t) \\
\frac{dI}{dt} &= g(S, I) - (d + \mu + \delta)I + \sigma_2 I w_2(t) \\
\frac{dR}{dt} &= \mu I - (d + \gamma)R + \sigma_3 + \sigma_3 R w_3(t) \\
g(S, I) &= \frac{kS^h I}{S^h + \alpha I^h} \\
b = 1, \quad d = 0.1, \quad k = 0.2, \quad \alpha = 0.5, \quad \gamma = 0.01, \quad \mu = 0.05 \\
\delta = 0.01, \quad h = 2, \quad \sigma_1 = 0.2, \quad \sigma_2 = 0.2, \quad \sigma_3 = 0.1.
\end{aligned} \tag{10}$$

The hidden physics is the infection transmission rate,  $g(S, I)$ , which plays a key role in determining disease spread dynamics in many epidemic models [17, 18, 48, 54, 67, 68, 69, 70]. The form of  $g(S, I)$  is widely considered to be unknown, and each of the above-listed references propose different versions of this function. We apply SPINN to Eq. (10) to learn (or reconstruct)  $g(S, I)$ . We chose this case study to demonstrate that SPINN can not only broadly learn drift and diffusion coefficients but also can learn specific unknown physics terms within complex SDEs.

The hidden physics  $g(S, I)$  only contributes to the deterministic dynamics (i.e.,  $f(x, g(x))$  in Eq. 1) and appears in the time evolution equations for both

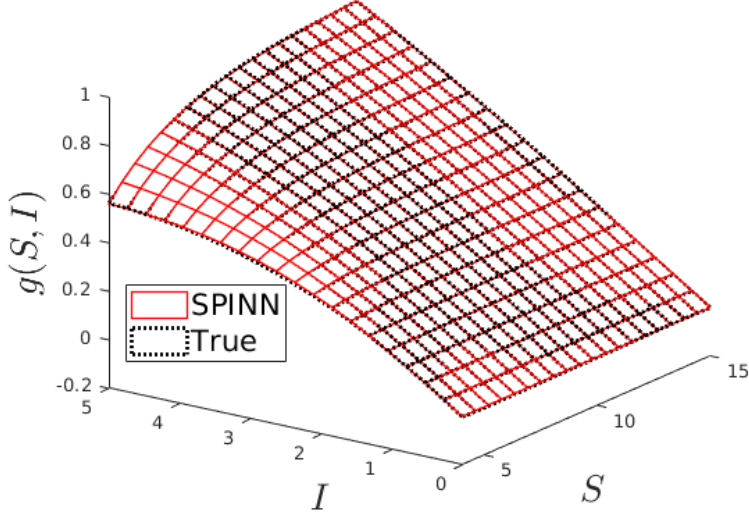


Figure 6: Learned hidden physics of susceptible-infectious-recovered (SIR) epidemic model. SPINN reconstructs  $g(S, I)$  with high accuracy.

$S$  and  $I$  in Eq. (10). The resulting loss function used to train  $g(S, I; \theta)$  is then given by:

$$\min_{\theta} \sum_{k=0}^K \left\| \hat{\mu}_S(t_k) - \mu_S(t_k) \right\|^2 + \left\| \hat{\mu}_I(t_k) - \mu_I(t_k) \right\|^2, \quad (11)$$

while the loss functions used to train  $g_1(x, u)$  and  $g_1(x_1, x_2)$  in the previous two case studies were given by Eq. (6).

Fig. 6 shows SPINN’s reconstruction of  $g(S, I)$ . SPINN learns  $g(S, I)$  with high accuracy and the reconstruction RMSE of  $g(S, I)$  is reported in Table 1 in Section 4. Fig. 7 plots the reconstruction RMSEs of hidden physics terms  $g_1(x_1, x_2)$  and  $g_2(x_1, x_2)$  from the Lotka-Volterra case study and  $g(S, I)$  from this case study against the total number of repeated state trajectories that were used to estimate moments  $\mu_x(t_k)$  and  $\Sigma_x(t_k)$ . Although each trajectory in case study was repeated  $10^5$  times to learn hidden physics (see Section 3 preamble), the RMSEs converge between  $10^3$  and  $10^4$  repeats. We expected  $g(S, I)$  to require fewer repeated state trajectories than  $g_1(x_1, x_2)$  and  $g_2(x_1, x_2)$  due to the fact that the loss function used to train  $g(S, I)$  contains more information (compare Eqs. (6) and (11)); however, this added

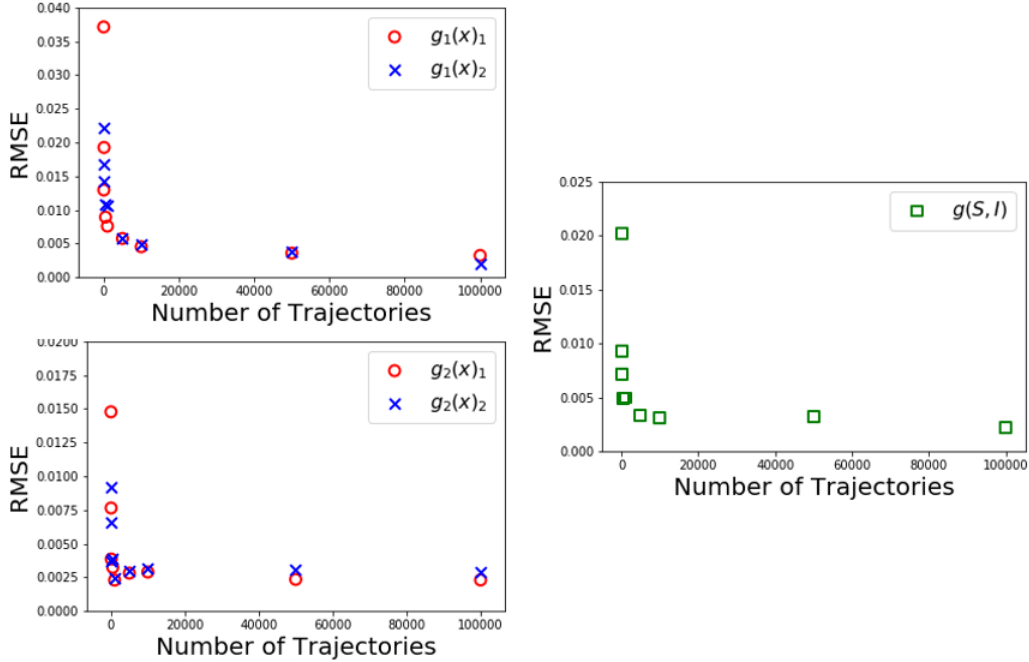


Figure 7: Sampling sensitivity analysis. The reconstruction root mean squared errors (RMSEs) of hidden physics terms  $g_1(x_1, x_2)$  and  $g_2(x_1, x_2)$  from the Lotka-Volterra case study and  $g(S, I)$  from the SIR case study are plotted against the total number of repeated state trajectories that were used to estimate moments  $\mu_x^i(t_j)$  from the collected data. Although each trajectory in case study was repeated  $10^5$  times to learn hidden physics, the RMSEs converge between  $10^3$  and  $10^4$  repeats.

information did not meaningfully impact the amount of required state trajectory repeats. We finally note that fewer replicates are likely required in systems with weaker noise terms.

#### 4. Conclusions and Future Work

We proposed a flexible and scalable moment-matching framework for training deep neural networks to learn constitutive equations that represent hidden physics within stochastic differential equations. We demonstrated the proposed stochastic physics-informed neural network framework on three benchmark *in-silico* case studies from the literature. We analyzed the performance of the proposed framework in terms of the choice of the uncertainty propagation strategy, hyper-parameter sensitivity, and the total number of repeated state trajectories required to accurately learn hidden

Case Study	Hidden Physics	RMSE
Colloidal Self-Assembly with UT	$g_1(x, u)$	$2.4 \times 10^{-4}$
Colloidal Self-Assembly with UT	$g_2(x, u)$	$4.35 \times 10^{-5}$
Colloidal Self-Assembly with Lin	$g_1(x, u)$	$1.40 \times 10^{-3}$
Colloidal Self-Assembly with Lin	$g_2(x, u)$	$4.18 \times 10^{-4}$
Lotka-Volterra	$g_1(x_1, x_2)_1$	$3.24 \times 10^{-3}$
Lotka-Volterra	$g_1(x_1, x_2)_2$	$2.01 \times 10^{-3}$
Lotka-Volterra	$g_2(x_1, x_2)_1$	$2.31 \times 10^{-3}$
Lotka-Volterra	$g_2(x_1, x_2)_2$	$2.91 \times 10^{-3}$
Susceptible-Infectious-Recovered	$g(S, I)$	$2.17 \times 10^{-3}$

Table 1: Reconstruction accuracy of learned hidden physics. The table shows the root mean squared errors (RMSEs) of the learned hidden physics in each case study in Sections 3.1 (colloidal self-assembly), 3.2 (Lotka-Volterra with coexistence equilibrium), and 3.3 (SIR). In each case, the RMSE is calculated by defining 100 evenly spaced points over each dimension and averaging the root of the squared error at each point. Note that in the case of colloidal self-assembly, UT and Lin refer to the uncertainty propagation techniques of unscented transform and linearization.

physics. We showed the framework’s scalability by learning highly nonlinear hidden physics within multidimensional stochastic differential equations with multiplicative noise. We illustrated the framework’s flexibility by (i) learning both general drift and diffusion coefficients and specific unknown functions within stochastic differential equations, (ii) incorporating different uncertainty propagation techniques into the framework, and (iii) analyzing the framework’s robustness to various hyper-parameter choices. An open challenge is the fact that a large number of repeated state trajectories are required to accurately learn hidden physics. We will focus future work on implementing more advanced sampling and optimization techniques to address this issue. We will additionally implement Bayesian optimization to more systematically select hyper-parameters and experiment with more advanced uncertainty propagation techniques.

## References

- [1] J. Honerkamp, Stochastic dynamical systems: concepts, numerical methods, data analysis, John Wiley & Sons, 1993.
- [2] N. G. Van Kampen, Stochastic differential equations, Physics reports 24 (3) (1976) 171–228.

- [3] N. G. Van Kampen, Stochastic processes in physics and chemistry, Vol. 1, Elsevier, 1992.
- [4] G. Volpe, J. Wehr, Effective drifts in dynamical systems with multiplicative noise: a review of recent progress, Reports on Progress in Physics 79 (5) (2016) 053901.
- [5] L. Arnold, Stochastic differential equations, New York (1974).
- [6] S. Schuster, M. Marhl, T. Höfer, Modelling of simple and complex calcium oscillations: From single-cell responses to intercellular signalling, European Journal of Biochemistry 269 (5) (2002) 1333–1355.
- [7] M. Pereyra, P. Schniter, E. Chouzenoux, J.-C. Pesquet, J.-Y. Tourneret, A. O. Hero, S. McLaughlin, A survey of stochastic simulation and optimization methods in signal processing, IEEE Journal of Selected Topics in Signal Processing 10 (2) (2015) 224–241.
- [8] P. C. Young, Stochastic, dynamic modelling and signal processing: time variable and state dependent parameter estimation, Nonlinear and non-stationary signal processing (2000) 74–114.
- [9] X. Tang, B. Rupp, Y. Yang, T. D. Edwards, M. A. Grover, M. A. Bevan, Optimal feedback controlled assembly of perfect crystals, ACS nano 10 (7) (2016) 6791–6798.
- [10] M. A. Bevan, D. M. Ford, M. A. Grover, B. Shapiro, D. Maroudas, Y. Yang, R. Thyagarajan, X. Tang, R. M. Sehgal, Controlling assembly of colloidal particles into structured objects: Basic strategy and a case study, Journal of Process Control 27 (2015) 64–75.
- [11] D. J. Beltran-Villegas, R. M. Sehgal, D. Maroudas, D. M. Ford, M. A. Bevan, A smoluchowski model of crystallization dynamics of small colloidal clusters, The Journal of chemical physics 135 (15) (2011) 154506.
- [12] D. J. Beltran-Villegas, R. M. Sehgal, D. Maroudas, D. M. Ford, M. A. Bevan, Colloidal cluster crystallization dynamics, The Journal of chemical physics 137 (13) (2012) 134901.
- [13] K. Singer, Application of the theory of stochastic processes to the study of irreproducible chemical reactions and nucleation processes, Journal

- of the Royal Statistical Society: Series B (Methodological) 15 (1) (1953) 92–106.
- [14] O. Penrose, Nucleation and droplet growth as a stochastic process, *Analysis and Stochastics of Growth Processes and Interface Models* (2008) 265.
  - [15] C. Zhu, G. Yin, On competitive lotka–volterra model in random environments, *Journal of Mathematical Analysis and Applications* 357 (1) (2009) 154–170.
  - [16] D. H. Nguyen, G. Yin, Coexistence and exclusion of stochastic competitive lotka–volterra models, *Journal of differential equations* 262 (3) (2017) 1192–1225.
  - [17] C. Bain, Applied mathematical ecology, *Journal of Epidemiology and Community Health* 44 (3) (1990) 254.
  - [18] A. Korobeinikov, P. K. Maini, Non-linear incidence and stability of infectious disease models, *Mathematical medicine and biology: a journal of the IMA* 22 (2) (2005) 113–128.
  - [19] Y. Gao, A. Gray, H. E. Tseng, F. Borrelli, A tube-based robust nonlinear predictive control approach to semiautonomous ground vehicles, *Vehicle System Dynamics* 52 (6) (2014) 802–823.
  - [20] D. Lamouroux, K. Lehnertz, Kernel-based regression of drift and diffusion coefficients of stochastic processes, *Physics Letters A* 373 (39) (2009) 3507–3512.
  - [21] J. Gottschall, J. Peinke, On the definition and handling of different drift and diffusion estimates, *New Journal of Physics* 10 (8) (2008) 083034.
  - [22] G. Hummer, Position-dependent diffusion coefficients and free energies from bayesian analysis of equilibrium and replica molecular dynamics simulations, *New Journal of Physics* 7 (1) (2005) 34.
  - [23] A. Ghysels, R. M. Venable, R. W. Pastor, G. Hummer, Position-dependent diffusion tensors in anisotropic media from simulation: oxygen transport in and through membranes, *Journal of chemical theory and computation* 13 (6) (2017) 2962–2976.

- [24] R. Friedrich, S. Siegert, J. Peinke, M. Siefert, M. Lindemann, J. Raethjen, G. Deuschl, G. Pfister, et al., Extracting model equations from experimental data, *Physics Letters A* 271 (3) (2000) 217–222.
- [25] H. Karimi, K. B. McAuley, Bayesian objective functions for estimating parameters in nonlinear stochastic differential equation models with limited data, *Industrial & Engineering Chemistry Research* 57 (27) (2018) 8946–8961.
- [26] D. Kleinhans, R. Friedrich, A. Nawroth, J. Peinke, An iterative procedure for the estimation of drift and diffusion coefficients of langevin processes, *Physics Letters A* 346 (1-3) (2005) 42–46.
- [27] S. Siegert, R. Friedrich, J. Peinke, Analysis of data sets of stochastic systems, *Physics Letters A* 243 (5-6) (1998) 275–280.
- [28] A. Shrestha, A. Mahmood, Review of deep learning algorithms and architectures, *IEEE Access* 7 (2019) 53040–53065.
- [29] R. Zhang, W. Li, T. Mo, Review of deep learning, arXiv preprint arXiv:1804.01653 (2018).
- [30] H. I. Fawaz, G. Forestier, J. Weber, L. Idoumghar, P.-A. Muller, Deep learning for time series classification: a review, *Data mining and knowledge discovery* 33 (4) (2019) 917–963.
- [31] M. Raissi, P. Perdikaris, G. E. Karniadakis, Physics-informed neural networks: A deep learning framework for solving forward and inverse problems involving nonlinear partial differential equations, *Journal of Computational Physics* 378 (2019) 686–707.
- [32] M. Raissi, A. Yazdani, G. E. Karniadakis, Hidden fluid mechanics: Learning velocity and pressure fields from flow visualizations, *Science* 367 (6481) (2020) 1026–1030.
- [33] Y. Yang, P. Perdikaris, Adversarial uncertainty quantification in physics-informed neural networks, *Journal of Computational Physics* 394 (2019) 136–152.
- [34] L. Yang, X. Meng, G. E. Karniadakis, B-pinns: Bayesian physics-informed neural networks for forward and inverse pde problems with noisy data, *Journal of Computational Physics* 425 (2021) 109913.

- [35] D. Zhang, L. Lu, L. Guo, G. E. Karniadakis, Quantifying total uncertainty in physics-informed neural networks for solving forward and inverse stochastic problems, *Journal of Computational Physics* 397 (2019) 108850.
- [36] A. R. Hall, et al., *Generalized method of moments*, Oxford university press, 2005.
- [37] L. Mátyás, C. Gourieroux, P. C. Phillips, et al., *Generalized method of moments estimation*, Vol. 5, Cambridge University Press, 1999.
- [38] J. M. Wooldridge, Applications of generalized method of moments estimation, *Journal of Economic perspectives* 15 (4) (2001) 87–100.
- [39] M. I. Ribeiro, Kalman and extended kalman filters: Concept, derivation and properties, *Institute for Systems and Robotics* 43 (2004) 46.
- [40] J. A. Paulson, M. Martin-Casas, A. Mesbah, Input design for online fault diagnosis of nonlinear systems with stochastic uncertainty, *Industrial & Engineering Chemistry Research* 56 (34) (2017) 9593–9605.
- [41] E. A. Wan, R. Van Der Merwe, The unscented kalman filter for nonlinear estimation, in: *Proceedings of the IEEE 2000 Adaptive Systems for Signal Processing, Communications, and Control Symposium (Cat. No. 00EX373)*, Ieee, 2000, pp. 153–158.
- [42] S. J. Julier, J. K. Uhlmann, New extension of the kalman filter to nonlinear systems, in: *Signal processing, sensor fusion, and target recognition VI*, Vol. 3068, International Society for Optics and Photonics, 1997, pp. 182–193.
- [43] A. G. Baydin, B. A. Pearlmutter, A. A. Radul, J. M. Siskind, Automatic differentiation in machine learning: a survey, *Journal of machine learning research* 18 (2018).
- [44] M. Abadi, P. Barham, J. Chen, Z. Chen, A. Davis, J. Dean, M. Devin, S. Ghemawat, G. Irving, M. Isard, et al., Tensorflow: A system for large-scale machine learning, in: *12th {USENIX} symposium on operating systems design and implementation ({OSDI} 16)*, 2016, pp. 265–283.

- [45] D. Shen, H. Wu, B. Xia, D. Gan, Polynomial chaos expansion for parametric problems in engineering systems: A review, *IEEE Systems Journal* 14 (3) (2020) 4500–4514.
- [46] X. Tang, Y. Xue, M. A. Grover, Colloidal self-assembly with model predictive control, in: *2013 American Control Conference, IEEE, 2013*, pp. 4228–4233.
- [47] J. Xiong, X. Li, H. Wang, The survival analysis of a stochastic lotka-volterra competition model with a coexistence equilibrium, *Mathematical Biosciences* 1 (k1k2) (2019) 1–k1k2.
- [48] Y. Cai, Y. Kang, W. Wang, A stochastic sirs epidemic model with non-linear incidence rate, *Applied Mathematics and Computation* 305 (2017) 221–240.
- [49] J. O’Leary, Stochastic physics-informed neural networks, <https://github.com/jtoleary/SPINN>, online; accessed 24 August 2021 (2021).
- [50] B. Peeters, G. De Roeck, Stochastic system identification for operational modal analysis: a review, *J. Dyn. Sys., Meas., Control* 123 (4) (2001) 659–667.
- [51] E. Reynders, System identification methods for (operational) modal analysis: review and comparison, *Archives of Computational Methods in Engineering* 19 (1) (2012) 51–124.
- [52] X. Hong, R. J. Mitchell, S. Chen, C. J. Harris, K. Li, G. W. Irwin, Model selection approaches for non-linear system identification: a review, *International journal of systems science* 39 (10) (2008) 925–946.
- [53] J. Schoukens, L. Ljung, Nonlinear system identification: A user-oriented road map, *IEEE Control Systems Magazine* 39 (6) (2019) 28–99.
- [54] I. Bauer, H. G. Bock, S. Körkel, J. P. Schlöder, Numerical methods for optimum experimental design in dae systems, *Journal of Computational and Applied mathematics* 120 (1-2) (2000) 1–25.
- [55] N. G. Van Kampen, Itô versus stratonovich, *Journal of Statistical Physics* 24 (1) (1981) 175–187.

- [56] A. J. Chorin, O. H. Hald, Stochastic tools in mathematics and science, Vol. 1, Springer, 2009.
- [57] J. M. Sancho, M. San Miguel, S. Katz, J. Gunton, Analytical and numerical studies of multiplicative noise, *Physical Review A* 26 (3) (1982) 1589.
- [58] P. E. Kloeden, E. Platen, Stochastic differential equations, in: *Numerical Solution of Stochastic Differential Equations*, Springer, 1992, pp. 103–160.
- [59] G. Mil'shtejn, Approximate integration of stochastic differential equations, *Theory of Probability & Its Applications* 19 (3) (1975) 557–562.
- [60] H. Janssen, Monte-carlo based uncertainty analysis: Sampling efficiency and sampling convergence, *Reliability Engineering & System Safety* 109 (2013) 123–132.
- [61] G. Hinton, N. Srivastava, K. Swersky, Neural networks for machine learning lecture 6a overview of mini-batch gradient descent, Cited on 14 (8) (2012) 2.
- [62] L. Prechelt, Early stopping-but when?, in: *Neural Networks: Tricks of the trade*, Springer, 1998, pp. 55–69.
- [63] D. P. Kingma, J. Ba, Adam: A method for stochastic optimization, arXiv preprint arXiv:1412.6980 (2014).
- [64] P. Ramachandran, B. Zoph, Q. V. Le, Searching for activation functions, arXiv preprint arXiv:1710.05941 (2017).
- [65] F. Chollet, et al., Keras, <https://github.com/fchollet/keras> (2015).
- [66] J. Snoek, H. Larochelle, R. P. Adams, Practical bayesian optimization of machine learning algorithms, *Advances in neural information processing systems* 25 (2012).
- [67] H. W. Hethcote, The mathematics of infectious diseases, *SIAM review* 42 (4) (2000) 599–653.

- [68] V. Capasso, G. Serio, A generalization of the kermack-mckendrick deterministic epidemic model, *Mathematical biosciences* 42 (1-2) (1978) 43–61.
- [69] W.-m. Liu, S. A. Levin, Y. Iwasa, Influence of nonlinear incidence rates upon the behavior of sirs epidemiological models, *Journal of mathematical biology* 23 (2) (1986) 187–204.
- [70] S. Yuan, B. Li, Global dynamics of an epidemic model with a ratio-dependent nonlinear incidence rate, *Discrete Dynamics in Nature and Society* 2009 (2009).